Available online at www.sciencedirect.com

ScienceDirect

Energy Procedia 45 (2014) 518 – 527

Energy Procedia

68th Conference of the Italian Thermal Machines Engineering Association, ATI2013

A comparison between high-order temporal integration methods applied to the Discontinuous Galerkin discretized Euler equations

Alessandra Nigro[a,*], Carmine De Bartolo[a], Salvatore M. Renda[a], Francesco Bassi[b]

[a] *University of Calabria-Department of Mechanical, Energetic and Management Engineering, Ponte P. Bucci cubo 44/C, Rende (CS) 87036, Italy*
[b] *University of Bergamo-Department of Industrial Engineering, Viale Marconi 5, Dalmine (BG) 24044, Italy*

Abstract

In this work we present a high-order Discontinuous Galerkin (DG) space approximation coupled with two high-order temporal integration methods for the numerical solution of time-dependent compressible flows. The time integration methods analyzed are the explicit Strong-Stability-Preserving Runge-Kutta (SSPRK) and the Two Implicit Advanced Step-point (TIAS) schemes. Their accuracy and efficiency are evaluated by means of an inviscid test case for which an exact solution is available. The study is carried out for several time-steps using different polynomial order approximations and several levels of grid refinement. The effect of mesh irregularities on the accuracy is also investigated by considering randomly perturbed meshes. The analysis of the results has the twofold objective of *(i)* assessing the performances of the temporal schemes in the context of the high-order DG discretization and *(ii)* determining if high-order implicit schemes can displace widely used high-order explicit schemes.

Selection and peer-review under responsibility of ATI NAZIONALE

Keywords: high-order, unsteady problems, Discontinuous Galerkin, Strong-Stability-Preserving Runge-Kutta, Two Implicit Advanced Step-point

1. Introduction

Computational Fluid Dynamics (CFD) has mainly focused on steady state problems, and even the more advanced CFD codes based on high-order spatial discretization are sometimes inefficient for unsteady computations requiring high accuracy. However, the solution of the unsteady phenomena is needed in many areas including turbomachinery and Internal Combustion Engine (ICE). In turbomachinery unsteady phenomena can be due, for example, to rotor/stator interaction, valve closure, formation of Karman vortex street and many others while ICE are characterized by highly unsteady phenomena of in-cylinder flows. The understanding of these complex unsteady flows must be improved to increase the efficiency of such systems.

Simulations of unsteadiness require high computing time, therefore high accurate time integration schemes are mandatory to perform efficient unsteady simulations and to capture the significant flow features of transient problems. Higher-order spatial schemes additionally contribute to time-dependent efficiency. The error at a specified final time

* Corresponding author. Tel.: +39-0984-494880 ; fax: +39-0984-494673
E-mail address: alessandra.nigro@unical.it

1876-6102
Selection and peer-review under responsibility of ATI NAZIONALE
doi:10.1016/j.egypro.2014.01.056

(global error) is the sum of the errors at each integration step (local error): the error accumulates linearly in time (see [1,2] for a detailed demonstration). The local error consists of three components: the temporal truncation error, the spatial truncation error and the algebraic error. A simulation requiring many time-steps to reach a numerical solution within the engineering accuracy (two to three significant digits) needs to be performed at extremely small local errors. High order schemes are the most efficient means of achieving the high levels of local accuracy required at each integration step [2].

Among the high-order spatial numerical schemes usually considered for the accurate and efficient solution of CFD problems, one of the most promising is the Discontinuous Galerkin (DG) finite elements method. Advantages and capabilities of DG methods are actively investigated in many different fields of computational physics, such as gas dynamics, compressible and incompressible flows, turbomachinery, magneto-hydrodynamics and many others. For a recent overview of DG methods we refer to [3]. The development of DG methods was mainly focused on the spatial discretization. The time discretization can be performed also by a discontinuous approximation [4,5], but the most usual approach is the application of the method of line in which the system of equations, resulting form the space discretization, is advanced in time with one of the time-integration methods developed for solving ordinary differential equations.

Two of the most widely used approaches for the numerical solution of unsteady flows are the high-order explicit Runge-Kutta methods [6–8] and the implicit Backward Differentiation Formulae (BDF) [9–11]. All these methods present advantages and limitations. Explicit Runge-Kutta schemes are high-order schemes easy to implement and parallelize, and require only limited memory storage. However, for problems requiring high spatial resolutions of very thin boundary layers and characterized by very stiff system of equations, the time step restriction would result in an inefficient time integration technique. In this regard, the class of Strong-Stability-Preserving Runge-Kutta (SSPRK) time discretization methods offers significant advantages as its better stability property enable the increase in the maximum allowable time step.

The implicit multi-step BDF schemes are very efficient for stiff initial-value problems but are not self-starting schemes and are *A*-stable only up to the second-order. Starting from the BDF approach, in order to obtain *A*-stable method with higher order of accuracy, the multi-step and multi-stage ideas have been combined in [12,13] to obtain Extended BDF (EBDF) and Modified Extended BDF (MEBDF) methods *A*-stable up to order 4, and in [14,15] to obtain Two Implicit Advanced Step-point (TIAS) algorithm *A*-stable up to order 6. On the other hand, implicit methods consist of one or more non-linear systems at each time-step, thus the use of efficient solution algorithms is required to make them competitive respect to explicit schemes.

The objective of this work is twofold: *(i)* to assess and investigate the performance of the explicit SSPRK and the implicit TIAS temporal schemes in the context of the high-order DG discretization and *(ii)* to determine if high-order implicit schemes can displace widely used high-order explicit schemes. The performances of the above temporal schemes have been evaluated by means of an inviscid isentropic convecting vortex aimed at testing the DG-SSPRK and DG-TIAS schemes capability to preserve vorticity in an unsteady inviscid flow. The study is carried out for several time-steps using different polynomial order approximations and several levels of grid refinement, considering also the effect of mesh irregularities on the accuracy of the results. Furthermore, long-time simulations are performed to clearly illustrate the advantages of the high-order time discretization.

In the following of the paper the governing equations and their DG space discretization are presented in Section 2. Section 3 is devoted to time discretizations. Numerical results are discussed in Section 4. Conclusions are reported in Section 5.

2. Governing equations and DG space discretization

The compressible Euler equations in conservative form based on the set of conservative variables $\mathbf{q} = [\rho, \rho u, \rho v, \rho E]^T$ are:

$$\frac{\partial \mathbf{q}}{\partial t} + \nabla \cdot \mathbf{F}_c(\mathbf{q}) = 0, \tag{1}$$

where $\mathbf{F}_c\left(\mathbf{f}_c, \mathbf{g}_c\right)$ is the inviscid flux vector given by:

$$\mathbf{f}_c = \begin{pmatrix} \rho u \\ \rho u^2 + p \\ \rho uv \\ \rho Hu \end{pmatrix}, \qquad \mathbf{g}_c = \begin{pmatrix} \rho v \\ \rho vu \\ \rho v^2 + p \\ \rho Hv \end{pmatrix}.$$

In these equations ρ is the fluid density, u and v are the x and y velocity components respectively and p is the pressure. E is the total internal energy for unit mass and the total enthalpy for unit mass is given by $H = E + p/\rho$.

In order to construct the DG discretization of Eq. (1), we consider an approximation Ω_h of the domain Ω consisting of a set of non-overlapping elements $\tau_h = \{K\}$, denoting by $\partial\Omega_h$ the boundary of the discrete approximation and by Γ_h^0 the set of internal edges. We consider piecewise polynomial functions on τ_h with no global continuity requirement. If $P_n\left(K\right)$ denotes the space of polynomial functions of degree at most n in the element K, and considering the function space:

$$\mathbf{V}_h = \{\mathbf{v}_h \in \left(L^2\left(\Omega_h\right)\right)^{N+2} : \mathbf{v}_h \in \left(P_n\left(K\right)\right)^{N+2} \forall K \in \tau_h\},$$

where N is the number of spatial dimensions, the DG formulation of Eq.(1) is then as follows: find $\mathbf{q}_h \in \mathbf{V}_h$ so that

$$\int_{\Omega_h} \mathbf{v}_h \cdot \frac{\partial \mathbf{q}_h}{\partial t} d\mathbf{x} - \int_{\Omega_h} \nabla \mathbf{v}_h : \mathbf{F}_c\left(\mathbf{q}_h\right) d\mathbf{x} + \int_{\Gamma_h^0} \left(\mathbf{v}_h^- - \mathbf{v}_h^+\right) \cdot \mathbf{H}\left(\mathbf{q}_h^+, \mathbf{q}_h^-, \mathbf{n}^-\right) d\sigma + \int_{\partial\Omega_h} \left(\mathbf{v}_h \otimes \mathbf{n}\right) : \mathbf{H}\left(\mathbf{q}_h^+, \mathbf{q}_h^b, \mathbf{n}\right) d\sigma = 0, \quad (2)$$

holds for an arbitrary test function $\mathbf{v}_h \in \mathbf{V}_h$. In this equation $(\cdot)^-$ and $(\cdot)^+$ symbols denote left and right state, see Fig. 1, and $\mathbf{H}\left(\mathbf{q}_h^+, \mathbf{q}_h^-, \mathbf{n}^-\right)$ and $\mathbf{H}\left(\mathbf{q}_h^+, \mathbf{q}_h^b, \mathbf{n}\right)$ are the numerical flux functions at the interior and boundary faces, respectively. For the inviscid numerical flux any of the numerical flux functions commonly considered in the finite volume method can be used. In the present work we employ the Godunov flux, i.e. the physical flux of the exact solution of a planar Riemann problem in the direction normal to the boundary.

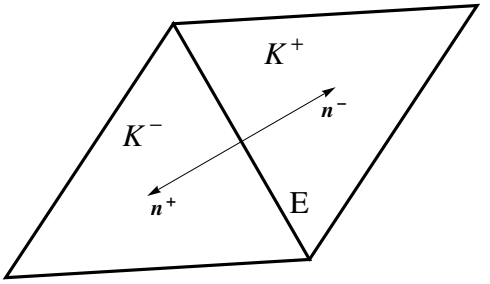

Fig. 1. Two elements K^+ and K^- sharing edge E.

3. Time discretization

The DG space discretization, Eq. (2), results in the following system of ordinary differential equations:

$$\mathbf{M}\frac{d\mathbf{Q}}{dt} + \mathbf{R}\left(\mathbf{Q}\right) = 0, \quad (3)$$

where $\mathbf{M}$ is the global block diagonal mass matrix, $\mathbf{Q}$ is the global vector of unknown degrees of freedom and $\mathbf{R}\left(\mathbf{Q}\right)$ is the vector of "residuals", i.e., the vector of nonlinear functions of $\mathbf{Q}$ resulting from the integrals of the DG discretized space differential operators in Eq. (2).

The above system is advanced in time with one of the time-integration methods developed for ordinary differential equations. In the following, the SSPRK and TIAS methods are briefly described.

- Strong-Stability-Preserving Runge Kutta (SSPRK) method.

  In Runge-Kutta schemes the solution is advanced in several stages and the residual is evaluated at intermediate states. The solution of the system (3) is advanced from time t to time $t + \Delta t$ applying the following expression:

$$\begin{aligned}
&\mathbf{q}^0 = \mathbf{q}^t, \\
&\mathbf{q}^i = \sum_{k=0}^{i-1} \alpha_{ik}\mathbf{q}^k + \beta_{ik}\Delta t\,(\mathbf{M})^{-1}\,\mathbf{R}\left(\mathbf{q}^k\right), \qquad i = 1, 2, ..., s. \\
&\mathbf{q}^{t+\Delta t} = \mathbf{q}^s,
\end{aligned}$$

  where i is the stage counter and α_{ik} and β_{ik}, are the multistage coefficients. These coefficients are used to weight the residual at each stage and can be optimized in order to expand the stability region of the scheme.
  The Runge-Kutta scheme employed in this work is the 5-stage fourth-order accurate SSP Runge-Kutta scheme, SSPRK (5,4). For further details about the coefficients of the optimal SSPRK (5,4) scheme we refer to [16].

- Two Implicit Advanced Step-point (TIAS) method.

  This new implicit multi-step scheme involves four stages: the first three are predictor stages that use a standard k-step BDF scheme, the last one is a corrector stage that uses an advanced implicit k-step formula of order $k+1$. The TIAS scheme was presented in [14,15] and the stability properties of this approach were investigated in detail in [17]. Assuming that approximate solutions $\mathbf{Q}_{n+j}$ have been calculated at t_{n+j} with $0 \le j \le k-1$, the general k-step TIAS algorithm of order $k+1$ consists of successively solving the following four stages to advance the solution in time:
  - Stage 1. Compute the first predictor $\bar{\mathbf{Q}}_{n+k}$ of order k with a k-step BDF:

$$\mathbf{M}\left(\bar{\mathbf{Q}}_{n+k} + \sum_{j=0}^{k-1} \hat{\alpha}_j \mathbf{Q}_{n+j}\right) + \Delta t\hat{\beta}_k \mathbf{R}\left(\bar{\mathbf{Q}}_{n+k}\right) = 0.$$

  - Stage 2. Compute the second predictor $\bar{\mathbf{Q}}_{n+k+1}$ of order k with a k-step BDF:

$$\mathbf{M}\left(\bar{\mathbf{Q}}_{n+k+1} + \hat{\alpha}_{k-1}\bar{\mathbf{Q}}_{n+k} + \sum_{j=0}^{k-2} \hat{\alpha}_j \mathbf{Q}_{n+j+1}\right) + \Delta t\hat{\beta}_k \mathbf{R}\left(\bar{\mathbf{Q}}_{n+k+1}\right) = 0.$$

  - Stage 3. Compute the third predictor $\bar{\mathbf{Q}}_{n+k+2}$ of order k with a k-step BDF:

$$\mathbf{M}\left(\bar{\mathbf{Q}}_{n+k+2} + \hat{\alpha}_{k-1}\bar{\mathbf{Q}}_{n+k+1} + \hat{\alpha}_{k-2}\bar{\mathbf{Q}}_{n+k} + \sum_{j=0}^{k-3} \hat{\alpha}_j \mathbf{Q}_{n+j+2}\right) + \Delta t\hat{\beta}_k \mathbf{R}\left(\bar{\mathbf{Q}}_{n+k+2}\right) = 0.$$

  - Stage 4. Compute the corrected solution $\mathbf{Q}_{n+k}$ of order $k+1$ using:

$$\begin{aligned}
&\mathbf{M}\left(\mathbf{Q}_{n+k} + \sum_{j=0}^{k-1} \tilde{\alpha}_j \mathbf{Q}_{n+j}\right) + \Delta t\Big[\tilde{\beta}_{k+2}\mathbf{R}\left(\bar{\mathbf{Q}}_{n+k+2}\right) + \tilde{\beta}_{k+1}\mathbf{R}\left(\bar{\mathbf{Q}}_{n+k+1}\right) + \beta_k \mathbf{R}\left(\bar{\mathbf{Q}}_{n+k}\right) \\
&+ \left(\tilde{\beta}_k - \beta_k\right)\mathbf{R}\left(\mathbf{Q}_{n+k}\right)\Big] = 0.
\end{aligned}$$

  In the first three stages $\hat{\alpha}_j$ and $\hat{\beta}_k$ are the BDF coefficients and in the last one $\tilde{\alpha}_j$, $\tilde{\beta}_{k+2}$, $\tilde{\beta}_{k+1}$, $\tilde{\beta}_k$ and β_k are the TIAS coefficients. In particular, $\tilde{\beta}_{k+2}$ and β_k are free coefficients which determine the stability properties of the scheme, while the other coefficients, expressed in terms of $\tilde{\beta}_{k+2}$, are determined such as the scheme has order

$k+1$. The residuals in stage 4 are computed once that each of the previous three stages has been solved:

$$\mathbf{R}\left(\bar{\mathbf{Q}}_{n+k}\right) = -\frac{\mathbf{M}}{\Delta t\hat{\beta}_k}\left(\bar{\mathbf{Q}}_{n+k} + \sum_{j=0}^{k-1}\hat{\alpha}_j\mathbf{Q}_{n+j}\right),$$

$$\mathbf{R}\left(\bar{\mathbf{Q}}_{n+k+1}\right) = -\frac{\mathbf{M}}{\Delta t\hat{\beta}_k}\left(\bar{\mathbf{Q}}_{n+k+1} + \hat{\alpha}_{k-1}\bar{\mathbf{Q}}_{n+k} + \sum_{j=0}^{k-2}\hat{\alpha}_j\mathbf{Q}_{n+j+1}\right),$$

$$\mathbf{R}\left(\bar{\mathbf{Q}}_{n+k+2}\right) = -\frac{\mathbf{M}}{\Delta t\hat{\beta}_k}\left(\bar{\mathbf{Q}}_{n+k+2} + \hat{\alpha}_{k-1}\bar{\mathbf{Q}}_{n+k+1} + \hat{\alpha}_{k-2}\bar{\mathbf{Q}}_{n+k} + \sum_{j=0}^{k-3}\hat{\alpha}_j\mathbf{Q}_{n+j+2}\right).$$

The TIAS scheme employed in this work is the 4-stage sixth-order accurate TIAS scheme, TIAS (4,6). For further details about the coefficients of TIAS (4,6) and the numerical techniques employed to improve the efficiency of the scheme we refer to [18].

4. Numerical results

In this section we present some numerical results demonstrating the performances of the proposed high-order DG-SSPRK and DG-TIAS schemes. The test case is an isentropic convecting vortex for which an exact solution is available. A uniform flow with a Mach number of $M_\infty = 0.05$ is perturbed by an isentropic vortex centered at (x_0, y_0). The resulting initial flow variables are:

$$u = u_\infty - \frac{(u_\infty\beta)\,(y-y_0)}{R}e^{-r^2/2},$$

$$v = \frac{(u_\infty\beta)\,(x-x_0)}{R}e^{-r^2/2},$$

$$T = T_\infty - \frac{1}{2}\frac{(\gamma-1)}{\gamma}\,(u_\infty\beta)^2\,e^{-r^2},$$

with $T_\infty = 1$, $u_\infty = M_\infty * \sqrt{\gamma}$, where $\gamma = 1.4$ is the ratio of specific heats of the fluid, $\beta = 0.02$, $R = 0.005$ and $r = \sqrt{(x-x_0)^2 + (y-y_0)^2}$ is the distance from the vortex center. The superposed vortex should be transported without distortion by the flow with a velocity of $(u_\infty, 0)$, thus the initial flow solution can be used to assess the accuracy of the computational method.

The vortex is initially placed at $(x_0, y_0) = (0.05, 0.05)$ in the domain $0 \le x \le 0.1$ and $0 \le y \le 0.1$. Periodic boundary conditions are set at top and bottom boundaries and at left and right boundaries, respectively. The test case has been computed on three successively refined uniform cartesian grids by using polynomial approximations from P^2 up to P^5. The grids are composed by 16×16 (coarse), 32×32 (medium) and 64×64 (fine) elements. The analysis is performed up to a final time corresponding to 50 periods T of vortex revolution. For each polynomial degree a temporal refinement study has been performed in order to determine the largest time-step value that ensures that the temporal discretization error does not affect the solution accuracy on a given mesh. Table 1 shows the appropriate time-step determined for each space discretization level and each temporal discretization algorithm. For the computations that refer to the SSPRK (5,4) method, exploiting the superior stability characteristics of this scheme with respect to other Runge-Kutta schemes, the CFL number has been set according to the rule:

$$\mathrm{CFL}_{RK\text{-}45} = 2 \cdot \frac{1}{2k+1},$$

where k is the degree of the polynomial approximation.

	TIAS (4,6)				SSPRK (5,4)			
Grid	P^2	P^3	P^4	P^5	P^2	P^3	P^4	P^5
Coarse	$T/40$	$T/80$	$T/160$	$T/320$	$T/1680$	$T/2400$	$T/3055$	$T/3735$
Medium	$T/80$	$T/160$	$T/320$	$T/640$	$T/3360$	$T/4800$	$T/6110$	$T/7470$
Fine	$T/160$	$T/320$	$T/640$	$T/1280$	$T/6720$	$T/9600$	$T/12220$	–

Table 1. Time-step size for different discretization levels as a function of the vortex period T.

In the following, we focus our attention on the u- and v-velocity components as this test case is aimed at testing the DG-SSPRK and DG-TIAS schemes capability to preserve vorticity in an unsteady inviscid flow. Figures 2 and 3 show the contour plots of u- and v-velocity components, respectively, after 50 periods T for P^2, P^3, P^4 and P^5 spatial discretizations obtained on the coarse grid using either the DG-SSPRK or DG-TIAS scheme. Overall it is evident that accuracy improves when higher-order spatial discretizations are employed. In particular, the higher-order P^5 scheme provides the best shape-retaining transport capability: the initial velocity component fields keep better their shapes. On the other hand, the figures show that by using the P^2 scheme the initial flow field is significantly diffused and dispersed. Note that the noisy patterns in Fig. 3 are associated with fluctuations in the v-velocity component ranging from order of 10^{-5} for the P^2 solution to order of 10^{-8} for the P^5 solution. These fluctuations reduce using the medium and the fine grids.

A more quantitative comparison is reported in Fig. 4, where the exact and the computed velocity component profiles along the $y = 0.05$ and $x = 0.05$ lines are shown for different spatial discretizations on the coarse grid. It can be observed that the use of P^5 scheme yielded very accurate solutions, even for very coarse grid size. Conversely, as showed for the velocity contours, the P^2 discretization produced the worst results.

The accuracy analysis is now extended for both the temporal schemes to the two successive levels of grid refinement by plotting the $L2$-norm errors of the u-velocity component versus $1/\sqrt{nDOFs}$, with $nDOFs$ equal to the total number of degrees of freedom per equation for the different spatial discretizations. Convergence histories are shown only for the u-velocity component as similar results are obtained for the v-velocity component. As expected, the left plot of Fig. 5 shows that the convergence histories computed using the DG-SSPRK and the DG-TIAS schemes are almost indistinguishable, with the higher-order discretizations achieving very low error levels. We remark that the DG-TIAS convergence histories have been obtained using time-step sizes considerably larger than those employed for the fourth-order accurate explicit scheme (see Table 1). For example to reach an accuracy level of order of 10^{-5} the implicit time-step size was 20 times bigger than the explicit one, while for an accuracy level of 10^{-7} this ratio increased to 30. On the other hand, the TIAS scheme consists of 4 non-linear systems at each time step, thus an efficiency study has been performed to evaluate if it outperforms the SSPRK method. To this purpose in the right plot of Fig. 5 the L2-norm of the error of the u-velocity component is plotted as a function of the computational cost expressed in work units for both the schemes and for different polynomial degrees. The work unit is defined as the ratio between the wall clock time taken by the DG-TIAS or DG-SSPRK solvers and that obtained using TauBench, an unstructured grid benchmark whose kernel is derived from Tau code [19]. The figure shows that the DG-TIAS scheme has a similar asymptotic behaviour of the Runge-Kutta scheme but it outperforms this one. For example, to achieve an accuracy level of order of 10^{-5} the DG-SSPRK scheme is about 3 times slower than the DG-TIAS scheme, while for an accuracy level of 10^{-7} this ratio reduces to 2.5.

A further analysis has been carried out by performing a new set of simulations on perturbed grids to investigate the effect of mesh irregularities on the accuracy of the proposed DG solvers. The perturbed meshes have been obtained from the corresponding cartesian ones randomly displacing the mesh's nodes, in both x- and y-coordinate directions, with a maximum distance $\delta_{max} = 0.15 \cdot h$, where h is the corresponding element size. Figure 6 shows the effect of the perturbation imposed on the 16 x 16 cartesian grid. The analysis has been restricted to the more efficient DG-TIAS scheme by using the same time steps of Table 1. The accuracy results are illustrated in the left plot of Fig. 7. The convergence histories and the error levels achieved on both the perturbed and the cartesian grids are very similar, even if P^4 and P^5 computations on the perturbed grids exhibit slopes reductions at approximately accuracy levels of 10^{-7} and 10^{-8}, respectively, thus demonstrating the robustness and the excellent dissipation property of the DG-TIAS solver. The right plot of Fig. 7 shows the L2-norm of the error of the u-velocity component as a function of the computational cost. The plot indicates that in order to reach an error level higher than 10^{-7} the perturbed computations

require the same computational cost of the regular-grid. For higher accuracy levels the computations on the cartesian grids outperform those on the perturbed ones due to their better asymptotic error reduction properties.

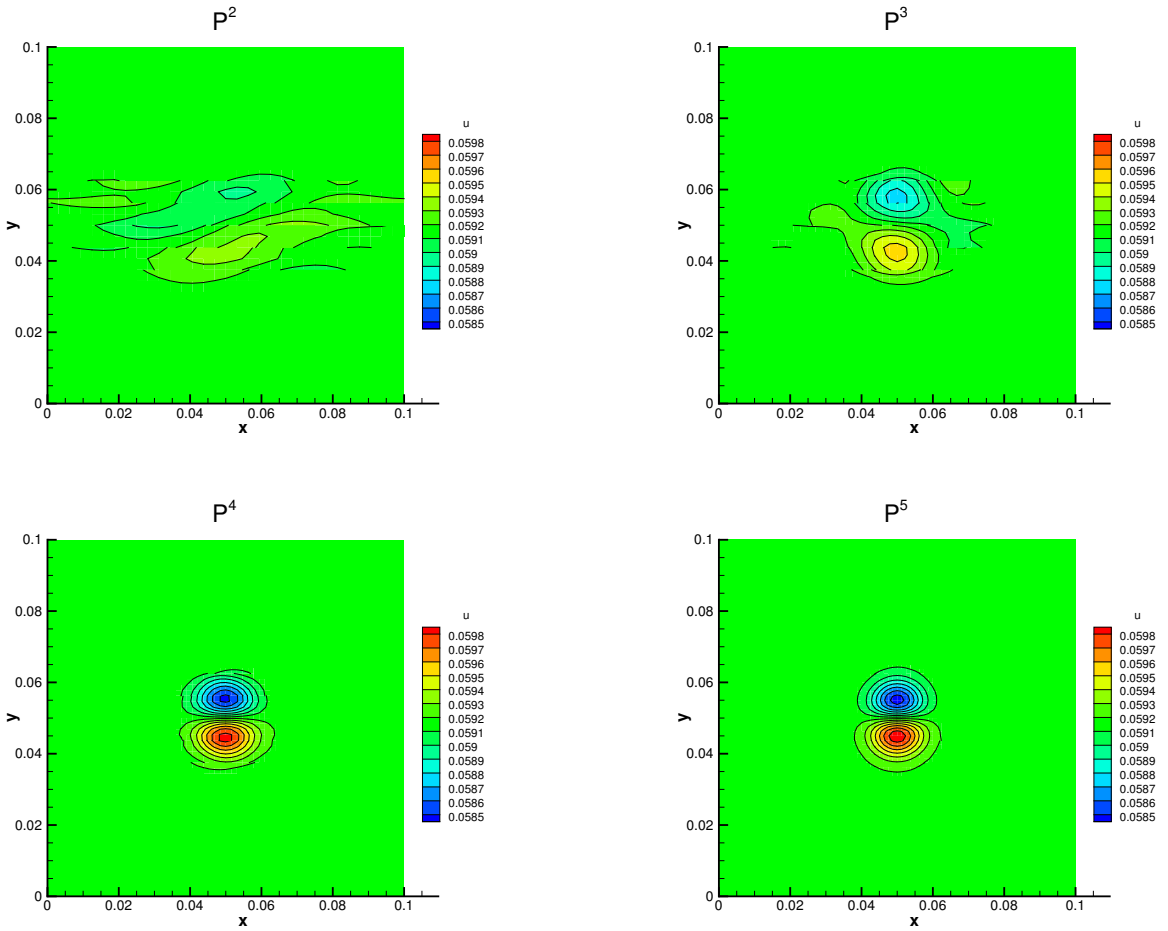

Fig. 2. *u*-velocity contours on the coarse grid for different DG spatial discretizations.

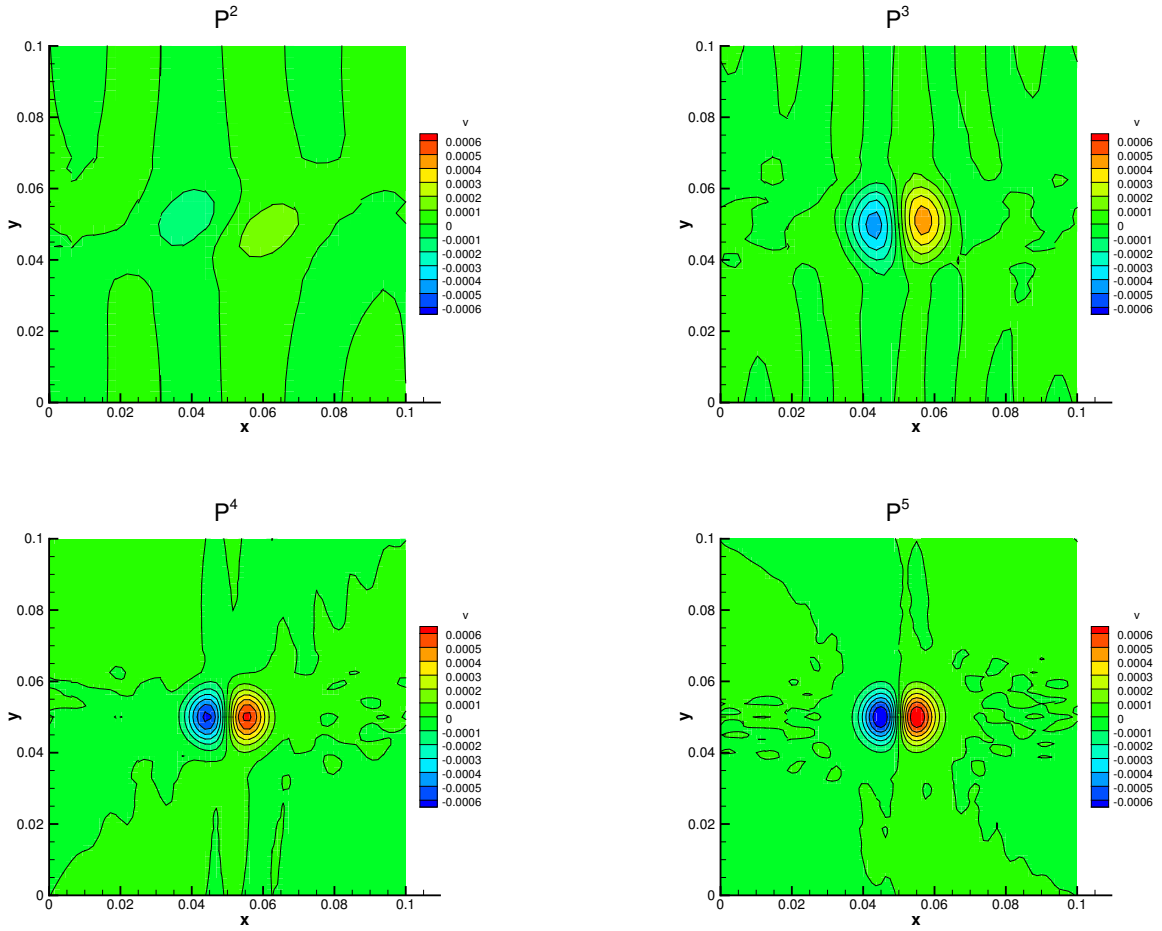

Fig. 3. v-velocity contours on the coarse grid for different DG spatial discretizations.

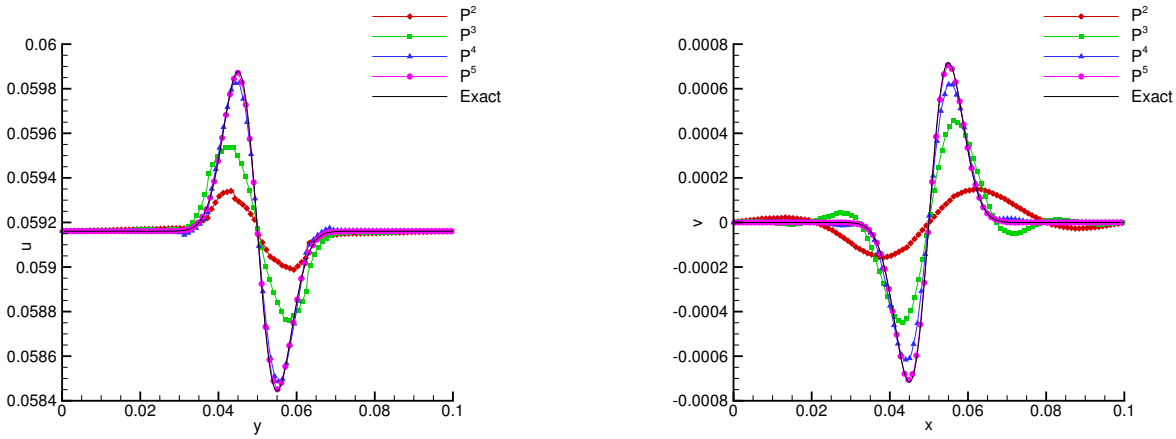

Fig. 4. u-velocity on the $x = 0.05$ line (left) and v-velocity on the $y = 0.05$ line (right) on the coarse grid for different DG discretizations.

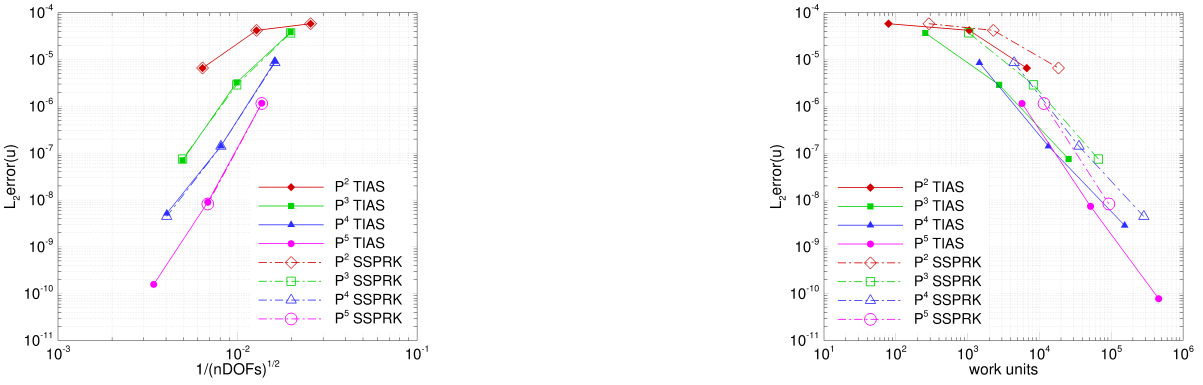

Fig. 5. L_2 error(u) as a function of $1/\sqrt{nDOFs}$ (left) and work units (right).

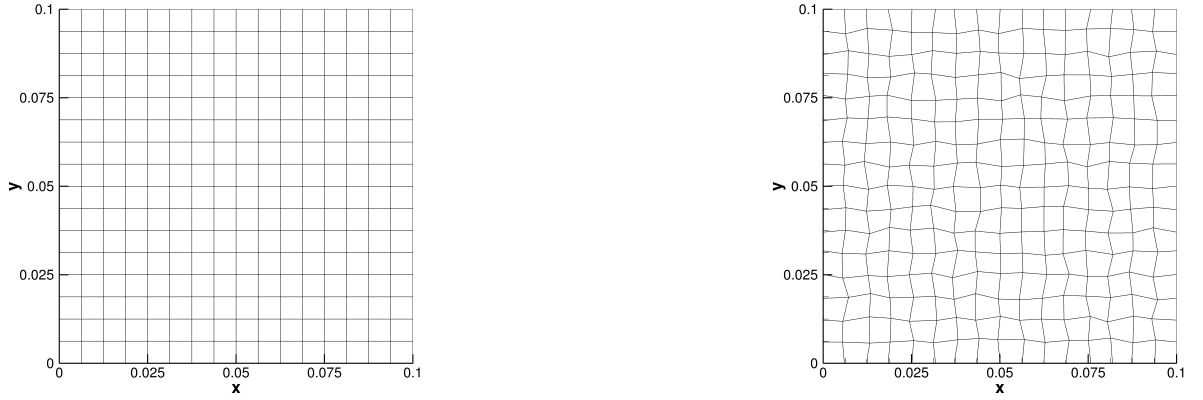

Fig. 6. 16×16 cartesian grid (left) and the corresponding randomly perturbed mesh (right).

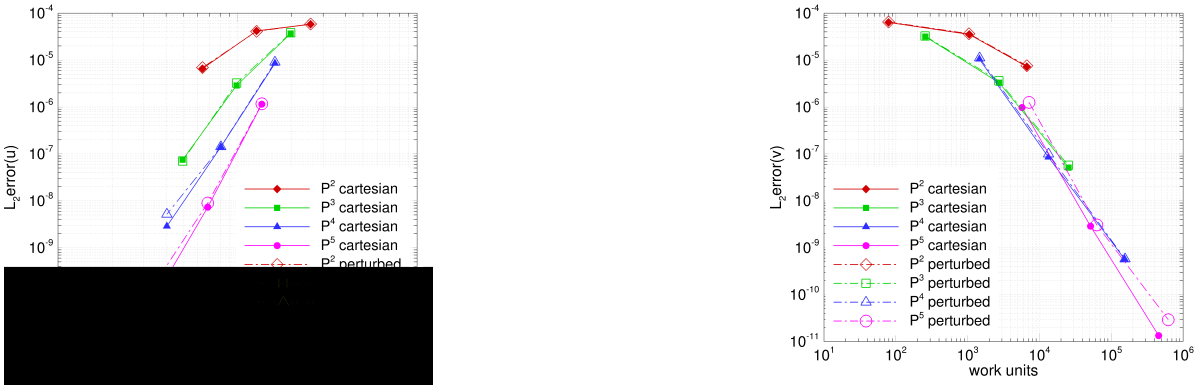

Fig. 7. L_2 error(u) as a function of $1/\sqrt{nDOFs}$ (left) and work units (right).

5. Conclusions

In this paper we have investigated the effectiveness of two high-order temporal integration methods for the numerical solution of time-dependent compressible inviscid flows. Space discretization is based on the high-order Discontinuous Galerkin method, while time integration has been performed employing an explicit and an implicit scheme. The explicit scheme is the 5-stage fourth-order accurate SSP Runge-Kutta scheme, SSPRK (5,4). The implicit scheme is the 4-stage sixth-order accurate TIAS scheme, TIAS (4,6). The performances of the two temporal schemes have been assessed by computing the convection of an isentropic vortex for several time-steps using different polynomial order approximations and several levels of grid refinement. The comparison of the computational efficiency of the two temporal scheme has shown that the computational effort required by TIAS (4,6) to achieve a given accuracy is at least 2.5 times lower than the one required by SSPRK (5,4). Furthermore the performance of the DG-TIAS(4,6) scheme has been evaluated for several perturbed grids, demonstrating the robustness and the excellent dissipative properties of the method. Ongoing work is devoted to the implementation of variable time step TIAS schemes.

References

[1] Kreiss H. O, Oliger J. Comparison of accurate methods for the integration of hyperbolic equations. *Tellus* 1972; 24:199–215.

[2] Carpenter M.H. , Singer B.A. , Yamaleev N. , Vatsa V.N. , Viken S.A., Atkins H.L. The current status of unsteady CFD approaches for aerodynamic flow control. AIAA Paper; No. 2002-3346 Presented at 1st AIAA Flow Control Conference, St. Louis, Missouri, June 24-26, 2002.

[3] Cockburn B., Karniadakis G., Shu C-W. The development of discontinuous Galerkin methods. *Discontinuous Galerkin Methods* 1999. In B. Cockburn, G. Karniadakis, and C.-W. Shu, Springer, 11:3–50

[4] Klaij C. M., van der Vegt J.J.W., Van der Ven H. Pseudo-time stepping for space-time discontinuous Galerkin discretizations of the compressible Navier-Stokes equations. *Journal of Computational Physics* 2006; 219(2):622–643.

[5] Lörcher F., Gassner G., Munz C. -D. A discontinuous Galerkin scheme based on a space-time expansion. I. Inviscid compressible flow in one space dimension. *Journal of Scientific Computing* 2007; 32(2):175–199.

[6] Bassi F., Rebay S. A high-order accurate discontinuous finite element method for the numerical solution of the compressible Navier-Stokes equations. *Journal of Computational Physics* 1997; 131(2):267–279.

[7] Cockburn B., Shu C.W. The Runge-Kutta Discontinuous Galerkin method for conservation laws V: Multidimensional systems. *Journal of Computational Physics* 1998; 141:199–224.

[8] Cockburn B., Shu C.W. Runge-Kutta Discontinuous Galerkin methods for convection dominated problems. *Journal of Scientific Computing* 2001; 16(3):173–261.

[9] Curtiss C. F., Hirschfelder J. O. Integration of stiff equation. Proc. Natl. Acad. Sci. USA 1952; 38: 235–243.

[10] Gear W. Simultaneous Numerical Solution of Differential Algebraic Equation. *IEEE Transaction on Circuit Theory* 1971; 18, 89-95.

[11] Ascher U., Petzold L. *Computer Method for Ordinary Differential Equations and Differential Algebraic Equations*. Siam; 1998.

[12] Cash J. R. On the Integration of Stiff Systems of O.D.E.s Using Extended Backward Differentiation Formulae. *Numerische Mathematik* 1980; 34: 235–246.

[13] Cash J. R. The integration of stiff initial value problems in ODEs using Modified Extended Backward Differentiation Formulae. *Computers & Mathematics with Applications* 1983; 9(5): 645–657.

[14] Psihoyios G. Advanced Step-point Methods for the Solution of Initial Value Problems. PhD Thesis, University of London - Imperial College of Science and Technology; 1995.

[15] Psihoyios G.Y., Cash J.R. A stability result for general linear methods with characteristic function having real poles only. *BIT Numerical Mathematics* 1998 (Springer, ISSN 00063835); 38(3): 612-617.

[16] Spiteri R.J., Ruuth S.J. A new class of optimal high-order strong-stability-preserving time discretization methods. *SIAM J. Numer. Anal.* 2002; 40(2): 469-491.

[17] Psihoyios G. A general formula for the stability functions of a group of Implicit Advanced Step-point (IAS) methods. *Mathematical and Computer Modelling* (Elsevier, ISSN 08957177) 2007;46 (1-2): 214-224.

[18] Nigro A., De Bartolo C., Bassi F. , Ghidoni A. High-order Discontinuous Galerkin solution of unsteady flows by using an advanced implicit method. Presented at: European workshop on High Order Nonlinear Numerical Methods for Evolutionary PDEs (HONOM 2013) , Bordeaux, France, March 18-22, 2013.

[19] www.ipacs-benchmark.org